Spectral Domain Analysis of Double Screen Frequency Selective Surfaces

Antonio Luiz Pereira de Siqueira Campos
Federal University of Rio Grande do Norte, Technological Center, Department of Communication Engineering, Av. Sen. Salgado Filho, 3000, Lagoa Nova, Natal – RN, Brazil, 59072-970, antonio.luiz@pq.cnpq.br
Tércio de Lima Silva
Federal Institute of Education, Science and Technology of Rio Grande do Norte, Campus Cidade Alta, Av. Rio Branco, 743, Centro, Natal – RN, Brazil, 59025-002, tlimas@bol.com.br

Abstract—**This paper presents a numerical investigation for a double screen frequency selective surface (FSS) with perfectly conducting rectangular patch elements. The analysis uses a full wave technique to obtain the scattering characteristics. The analysis combines the immitance approach and the method of moments to obtain the scattered fields and, consequently, the scattering characteristics of the structure. For validation of the analysis, numerical results are compared with measured and numerical results presented by another authors. A good agreement was obtained with experimental results.**

Index Terms — FSS, Spectral Domain Analysis, Double Screen FSS, Method of Moments, Immitance Approach.

I. INTRODUCTION

Frequency selective surfaces (FSS) have a large number of applications that contribute significantly to improving the performance of communications circuits. The issue of bandwidth has been one of the problems in the theory of FSS. One solution found to solve this problem is to use cascading or multilayered structures [1]. Many authors have used cascading FSS to obtain specific applications that require a higher bandwidth of operation [2] – [4].

Analysis of cascading FSS can be divided into two general categories: exact methods [5] – [7] and approximate methods [8] – [12]. Exact methods typically use some full wave analysis technique to find transmission and reflection characteristics of periodic structures [5].

In [13], the authors proposed a Fabry Perot Interferometer approach to obtain the scattering characteristics of a double screen FSS for TM incidence. This is an approximate analysis and produces good results when compared with measurements.

Electromagnetic performance parameters for a double screen FSS using double square loops was performed in [14]. The idea was use the equivalent circuit model with equivalent transmission line method to design a radome to operate in X-band.

In [15] the authors use the spectral domain analysis to obtain the scattering characteristics for a single layer FSS and, after this, they use an approximated technique to combine the responses of the single layer FSS to obtain the scattering parameters for a double screen FSS.

In this work, we propose the use of the spectral domain analysis that combine the immitance approach and the method of moments to obtain the scattering characteristics for double screen FSS structures. The advantage of this technique is that it allows obtain more accurate results when compared with approximated techniques. Numerical results are compared with experimental and numerical results presented in [15]. In [15] the authors use the spectral domain analysis to analyze the single FSS and then apply the approximate technique of the scattering matrix to analyze the FSS double screen. In this work, we analyze the double screen FSS using the spectral domain analysis.

II. FORMULATION

We start the formulation from the equations that determine the reflected and transmitted characteristics of a generalized periodic array [5].

$$R_{mn}^{TE} = \frac{j\left(\beta_n(\tilde{E}_{xt}^s + E_x^r \delta_{mn}) - \alpha_m(\tilde{E}_{yt}^s + E_y^r \delta_{mn}) \right)}{(\alpha_m^2 + \beta_n^2)} \tag{1}$$

$$T_{mn}^{TE} = \frac{j\left(\beta_n(\tilde{E}_{xb}^s + E_x^t \delta_{mn}) - \alpha_m(\tilde{E}_{yb}^s + E_y^t \delta_{mn}) \right)}{(\alpha_m^2 + \beta_n^2)} \tag{2}$$

where,

$$\gamma_{mn} = \sqrt{\alpha_{mn}^2 + \beta_{mn}^2 - k_0^2} \tag{3}$$

$$\delta_{mn} = \begin{cases} 1 & \text{if } m = n = 0 \\ 0 & \text{if } m \neq n \end{cases} \tag{4}$$

The superscripts b and t in the scattered field ($\tilde{E}^S$) are related to fields in top and bottom of the structure, respectively. The fields E^r and E^t are the complementary reflected and transmitted fields. The scattered fields are obtained from:

$$\begin{bmatrix} \tilde{E}_{xt,b}^s \\ \tilde{E}_{yt,b}^s \end{bmatrix} = \begin{bmatrix} \tilde{Z}_{xxt,b}^1 & \tilde{Z}_{xyt,b}^1 \\ \tilde{Z}_{yxt,b}^1 & \tilde{Z}_{yyt,b}^1 \end{bmatrix} \begin{bmatrix} \tilde{J}_x^1 \\ \tilde{J}_y^1 \end{bmatrix} + \begin{bmatrix} \tilde{Z}_{xxt,b}^2 & \tilde{Z}_{xyt,b}^2 \\ \tilde{Z}_{yxt,b}^2 & \tilde{Z}_{yyt,b}^2 \end{bmatrix} \begin{bmatrix} \tilde{J}_x^2 \\ \tilde{J}_y^2 \end{bmatrix} \tag{5}$$

where the superscripts *1* and *2* are related with the patch elements on dielectric layers *2* and *4*, as we can see in Figure 1.

The next step is to find the components of the Dyadic Green's function at interfaces *1-2* and *3-4*. These components are obtained as:

$$\begin{bmatrix} \tilde{Z}_{xx}^{1,2} & \tilde{Z}_{xy}^{1,2} \\ \tilde{Z}_{yx}^{1,2} & \tilde{Z}_{yy}^{1,2} \end{bmatrix} = \frac{1}{\alpha^2 + \beta^2} \begin{bmatrix} \beta^2 \tilde{Z}_{1,2}^{TM} + \alpha^2 \tilde{Z}_{1,2}^{TE} & \alpha\beta\left(\tilde{Z}_{1,2}^{TE} - \tilde{Z}_{1,2}^{TM} \right) \\ \alpha\beta\left(\tilde{Z}_{1,2}^{TE} - \tilde{Z}_{1,2}^{TM} \right) & \beta^2 \tilde{Z}_{1,2}^{TE} + \alpha^2 \tilde{Z}_{1,2}^{TM} \end{bmatrix} \tag{6}$$

where,

$$\tilde{Z}_{1,2}^{TM,TE} = \frac{1}{Y_{1,2+}^{e,h} + Y_{1,2-}^{e,h}} \tag{7}$$

Fig. 1. Double screen FSS considered in analysis.

To obtain the admittances $Y_{1,2+}^{e,h}$ and $Y_{1,2-}^{e,h}$ we will use the equivalent transmission line method [5].

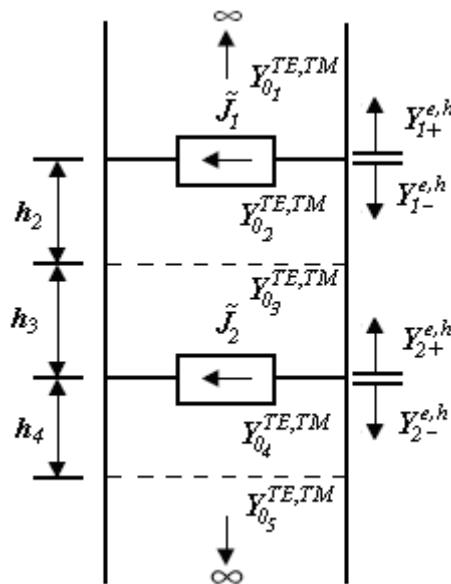The structure in Figure 1 will be represented by the circuit shown in Figure 2.

Fig. 2. Equivalent circuit to the structure considered in analysis.

For isotropic materials we define:

$$Y_{0i}^{TE} = \frac{\gamma_i}{j\omega\mu_0} \tag{8}$$

$$Y_{0i}^{TM} = \frac{j\omega\varepsilon_0\varepsilon_{ri}}{\gamma_i} \tag{9}$$

$$\gamma_i = \sqrt{\alpha_{mn}^2 + \beta_{mn}^2 - \omega^2\mu_0\varepsilon_0\varepsilon_{ri}} \tag{10}$$

where $i = 1, 2, \ldots, 5$.

The admittances $Y_{1,2+}^{e,h}$ and $Y_{1,2-}^{e,h}$ are the input admittances seen by the sources *1* and *2* in positive

and negative directions of *z* plane. The input admittance of a medium is given as:

$$Y_{in} = Y_0 \frac{Y_0 + Y_L \, coth(\gamma h)}{Y_L + Y_0 \, coth(\gamma h)} \tag{11}$$

where Y_0 is the characteristic admittance of the medium and Y_L is the load admittance of the medium.

The admittances $Y_{1+}^{e,h}$ and $Y_{1-}^{e,h}$ are obtained turn off the current source $\tilde{J}_2$, substituting it by an open circuit. In an analog way, the admittances $Y_{2+}^{e,h}$ and $Y_{2-}^{e,h}$ are obtained turn off the current source $\tilde{J}_1$. Applying (11) in the circuit of Figure 2, we obtain the admittances $Y_{1+}^{e,h}$ and $Y_{1-}^{e,h}$ as:

$$Y_{1+}^{e,h} = Y_{01}^{TM,TE} \tag{12}$$

$$Y_{1-}^{e,h} = Y_{02}^{TM,TE} \frac{Y_{02}^{TM,TE} + Y_{L2} \, coth(\gamma_2 h_2)}{Y_{L2} + Y_{02}^{TM,TE} \, coth(\gamma_2 h_2)} \tag{13}$$

$$Y_{L2} = Y_{03}^{TM,TE} \frac{Y_{03}^{TM,TE} + Y_{L3} \, coth(\gamma_0 h_3)}{Y_{L3} + Y_{03}^{TM,TE} \, coth(\gamma_0 h_3)} \tag{14}$$

$$Y_{L3} = Y_{04}^{TM,TE} \frac{Y_{04}^{TM,TE} + Y_{L4} \, coth(\gamma_4 h_4)}{Y_{L4} + Y_{04}^{TM,TE} \, coth(\gamma_4 h_4)} \tag{15}$$

$$Y_{L4} = Y_{05}^{TM,TE} \tag{16}$$

Applying (11) for the current source 2 in the circuit of Figure 2, we obtain the admittance $Y_{2+}^{e,h}$ as:

$$Y_{2+}^{e,h} = Y_{03}^{TM,TE} \frac{Y_{03}^{TM,TE} + Y_{L3} \, coth(\gamma_0 h_3)}{Y_{L3} + Y_{03}^{TM,TE} \, coth(\gamma_0 h_3)} \tag{17}$$

$$Y_{L3} = Y_{02}^{TM,TE} \frac{Y_{02}^{TM,TE} + Y_{L2} \, coth(\gamma_2 h_2)}{Y_{L2} + Y_{02}^{TM,TE} \, coth(\gamma_2 h_2)} \tag{18}$$

$$Y_{L2} = Y_{01}^{TM,TE} \tag{19}$$

We obtain the admittance $Y_{2-}^{e,h}$ as:

$$Y_{2-}^{e,h} = Y_{04}^{TM,TE} \frac{Y_{04}^{TM,TE} + Y_{L4} \, coth(\gamma_4 h_4)}{Y_{L4} + Y_{04}^{TM,TE} \, coth(\gamma_4 h_4)} \tag{20}$$

In (5), $\tilde{J}_1$ and $\tilde{J}_2$ are the current density components in the Fourier domain induced on the patches by the incident fields. These induced Fourier transformed current density components are expressed in terms of a set of basis function $\vec{f}_i$ as:

$$\vec{J} = \sum_i C_i \vec{f}_i \tag{21}$$

Considering the patches perfectly conducting we have:

$$\vec{E}^s + \vec{E}^i = 0 \tag{22}$$

These unknown coefficients for $\tilde{J}_1$ and $\tilde{J}_2$ can be obtained by the incident fields at the planes $z = 0$ and $z = -z_2$ as we can see in Figure 3.
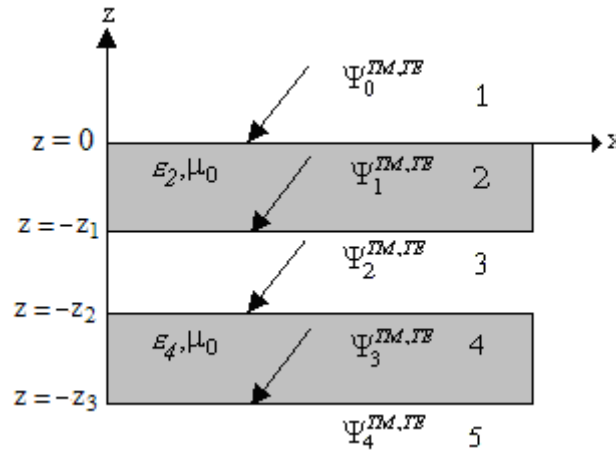
Fig. 3. Incident potentials on conducting patches.

In according with [3] the incident potentials are given as:

$$\Psi_o^{TE} = e^{j\alpha_0 x} e^{j\beta_0 y} e^{\gamma_0 z} + R e^{j\alpha_0 x} e^{j\beta_0 y} e^{-\gamma_0 z} \tag{23}$$

$$\Psi_1^{TE} = e^{j\alpha_0 x} e^{j\beta_0 y} \left[C_{11} cosh(\gamma_2 z_1) - C_{12} senh(\gamma_2 z_1) \right] \tag{24}$$

$$\Psi_2^{TE} = e^{j\alpha_0 x} e^{j\beta_0 y} \left[C_{21} cosh(\gamma_0 z_2) - C_{22} senh(\gamma_0 z_2) \right] \tag{25}$$

$$\Psi_3^{TE} = e^{j\alpha_0 x} e^{j\beta_0 y} \left[C_{31} cosh(\gamma_4 z_3) - C_{32} senh(\gamma_4 z_3) \right] \tag{26}$$

$$\Psi_4^{TE} = T e^{j\alpha_0 x} e^{j\beta_0 y} e^{\gamma_0 z} \tag{27}$$

To guarantee the continuity of the tangential fields at the dielectric interfaces, the incident fields are given as [3]:

$$E_x^i = -\frac{\partial \Psi_{i-1}^{TE}}{\partial y} \tag{28}$$

$$E_y^i = \frac{\partial \Psi_{i-1}^{TE}}{\partial x} \tag{29}$$

$$H_x^i = \frac{1}{j\omega\mu_0} \frac{\partial^2 \Psi_{i-1}^{TE}}{\partial x \partial z} \tag{30}$$

$$H_y^i = \frac{1}{j\omega\mu_0} \frac{\partial^2 \Psi_{i-1}^{TE}}{\partial y \partial z} \tag{31}$$

So, to determine the unknown coefficients of the basis functions, we need the incident fields at planes $z = 0$ and $z = z_2$, using (28) to (31) and applying conditions of continuity in these planes we obtain:

For z = 0:

$$\begin{bmatrix} E_{1x}^{inc} \\ E_{1y}^{inc} \end{bmatrix} = j \left(\frac{2\gamma_0}{\gamma_0 + \gamma_2 F_3} \right) e^{j\alpha_0 x} e^{j\beta_0 y} \begin{bmatrix} -\beta_0 \\ \alpha_0 \end{bmatrix} \tag{32}$$

For $z = -z_2$:

$$\begin{bmatrix} E_{2x}^{inc} \\ E_{2y}^{inc} \end{bmatrix} = j\left[coth(\gamma_0 z_2) - F_2 \right]\left(\frac{2\gamma_0 / \sinh(\gamma_0 z_2)}{\gamma_0 + \gamma_2 F_3} \right)(A_1 + B_1 F_3)e^{j\alpha_0 x}e^{j\beta_0 y}\begin{bmatrix} -\beta_0 \\ \alpha_0 \end{bmatrix} \tag{33}$$

where

$$F_3 = \frac{F_2 A_1 - C_1}{D_1 - F_2 B_1}$$

$$F_2 = \frac{F_1 A_2 - C_2}{D_2 - F_1 B_2}$$

$$F_1 = \frac{\gamma_4 + \gamma_0 \, coth(\gamma_4 z_3)}{\gamma_0 + \gamma_4 \, coth(\gamma_4 z_3)}$$

$$A_1 = cosh(\gamma_0 z_1)cosh(\gamma_2 z_1) - \frac{\gamma_2}{\gamma_0}sinh(\gamma_0 z_1)sinh(\gamma_2 z_1)$$

$$B_1 = -cosh(\gamma_0 z_1)sinh(\gamma_2 z_1) + \frac{\gamma_2}{\gamma_0}sinh(\gamma_0 z_1)cosh(\gamma_2 z_1)$$

$$C_1 = sinh(\gamma_0 z_1)cosh(\gamma_2 z_1) - \frac{\gamma_2}{\gamma_0}cosh(\gamma_0 z_1)sinh(\gamma_2 z_1)$$

$$D_1 = -sinh(\gamma_0 z_1)sinh(\gamma_2 z_1) + \frac{\gamma_2}{\gamma_0}cosh(\gamma_0 z_1)cosh(\gamma_2 z_1)$$

$$A_2 = cosh(\gamma_4 z_2)cosh(\gamma_0 z_2) - \frac{\gamma_0}{\gamma_4}sinh(\gamma_4 z_2)sinh(\gamma_0 z_2)$$

$$B_2 = -cosh(\gamma_4 z_2)sinh(\gamma_0 z_2) + \frac{\gamma_0}{\gamma_4}sinh(\gamma_4 z_2)cosh(\gamma_0 z_2)$$

$$C_2 = sinh(\gamma_4 z_2)cosh(\gamma_0 z_2) - \frac{\gamma_0}{\gamma_4}cosh(\gamma_4 z_2)sinh(\gamma_0 z_2)$$

$$D_2 = -sinh(\gamma_4 z_2)sinh(\gamma_0 z_2) + \frac{\gamma_0}{\gamma_4}cosh(\gamma_4 z_2)cosh(\gamma_0 z_2)$$

where $z_1 = h_2$, $z_2 = h_2 + h_3$, and $z_3 = h_2 + h_3 + h_4$.

The unknown coefficients of the basis functions can be obtained numerically from (30) and (31) as:

$$-\begin{bmatrix} E_{ix}^{inc} \\ E_{iy}^{inc} \end{bmatrix} = \sum_{q=1}^{2}\sum_{m=-\infty}^{\infty}\sum_{n=-\infty}^{\infty}\begin{bmatrix} \tilde{Z}_{xx}^{qi} & \tilde{Z}_{xy}^{qi} \\ \tilde{Z}_{yx}^{qi} & \tilde{Z}_{yy}^{qi} \end{bmatrix}\begin{bmatrix} \tilde{J}_{qx}(\alpha_{mn},\beta_{mn}) \\ \tilde{J}_{qy}(\alpha_{mn},\beta_{mn}) \end{bmatrix}e^{j(\alpha_{mn}x+\beta_{mn}y)} \tag{34}$$

where $i = 1, 2$.

The spectral variables, α_{mn} and β_{mn}, are defined as:

$$\alpha_{mn} = \frac{2\pi m}{T} + k_0 \, sen(\theta)cos(\phi) \tag{35}$$

$$\beta_{mn} = \frac{2\pi n}{T} + k_0 \, sen(\theta)sen(\phi) \tag{36}$$

where T is the periodicity of the unit cells in x and y directions. The angles θ and ϕ are the incidence angles and k_0 is the wave number in free space.

As we can see in (1) and (2), the transmission and reflection coefficients have terms of reflected and transmitted fields that are included when $m = n = 0$.

For the structure shown in Fig. 1, those reflected and transmitted fields are given as:

$$\tilde{E}_x^r = -j\beta_0 R \tag{37}$$

$$\tilde{E}_y^r = j\alpha_0 R \tag{38}$$

$$\tilde{E}_x^t = -j\beta_0 T e^{-\gamma_0 z_3} \tag{39}$$

$$\tilde{E}_y^t = j\alpha_0 T e^{-\gamma_0 z_3} \tag{40}$$

These coefficients are obtained during the procedure to determine the incident fields. They are given as:

$$R = \frac{\gamma_0 - \gamma_2 F_3}{\gamma_0 + \gamma_2 F_3} \tag{41}$$

$$T = (F_4 - F_5)\left(\frac{2\gamma_0 / \sinh(\gamma_4 z_3)}{\gamma_0 + \gamma_2 F_3}\right)e^{\gamma_0 z_3} \tag{42}$$

F_3 was defined earlier and F_4 and F_5 are given as:

$$F_4 = (A_1 A_2 + B_1 A_2 F_3 + C_1 B_2 + D_1 B_2 F_3)\coth(\gamma_4 z_3)$$

$$F_5 = A_1 C_2 + B_1 C_2 F_3 + C_1 D_2 + D_1 D_2 F_3$$

To finish the formulation, we need to know that when the scattered fields are evaluated at a distance h from the current source as depicted in Figure we need to modify (7). To transfer the impedances $Z^{TM,TE}$ to a distance h we need to multiply (7) by the factor:

$$Y_{transfer} = \frac{Y_0}{Y_0 \cos(\gamma h) + Y_L \sin(\gamma h)} \tag{43}$$

Therefore,

$$\tilde{Z}_{1,2}^{TM,TE} = \frac{1}{Y_{1,2+}^{e,h} + Y_{1,2-}^{e,h}} Y_{transfer} \tag{44}$$

If the scattered fields are evaluated two layers from the source we need to multiply (44) by (43) with Y_L, Y_0, γ and h replaced by the new ones.

To obtain the scattered fields at the top of the structure, we need to transfer $\tilde{Z}_2^{TM,TE}$ as:

$$\tilde{Z}_2^{TM,TE} = \frac{1}{Y_{2+}^{e,h} + Y_{2-}^{e,h}} Y_{transfer}^1 Y_{transfer}^2 \tag{45}$$

where,

$$Y_{transfer}^1 = \frac{Y_{03}}{Y_{03}\cos(\gamma_0 h_3) + Y_{L3}\sin(\gamma_0 h_3)} \tag{46}$$

$$Y_{transfer}^2 = \frac{Y_{02}}{Y_{02}\cos(\gamma_2 h_2) + Y_{L2}\sin(\gamma_2 h_2)} \tag{47}$$

where $Y_{0i}^{TM,TE}$, Y_{L2} and Y_{L3} were defined in (8), (9), (19) and (20), respectively.

To obtain the scattered fields at the top of the structure, we need to transfer the impedances as:

$$\tilde{Z}_1^{TM,TE} = \frac{1}{Y_{1+}^{e,h} + Y_{1-}^{e,h}} Y_{transfer}^1 Y_{transfer}^2 Y_{transfer}^3 \tag{48}$$

where,

$$Y_{transfer}^1 = \frac{Y_{02}}{Y_{02}\cos(\gamma_2 h_2) + Y_{L2}\sin(\gamma_2 h_2)} \tag{48}$$

$$Y_{transfer}^2 = \frac{Y_{03}}{Y_{03}\cos(\gamma_0 h_3) + Y_{L3}\sin(\gamma_0 h_3)} \tag{48}$$

$$Y_{transfer}^3 = \frac{Y_{04}}{Y_{04}\cos(\gamma_4 h_4) + Y_{L4}\sin(\gamma_4 h_4)} \tag{48}$$

The admittances Y_{L2}, Y_{L3} and Y_{L4} were defined in (13), (14) and (15), respectively.

For the current source *2* we have:

$$\tilde{Z}_2^{TM,TE} = \frac{1}{Y_{2+}^{e,h} + Y_{2-}^{e,h}} Y_{transfer}^1 \tag{49}$$

where $Y_{transfer}^1$ is the same of (48).

III. RESULTS

To validate our analysis, we compare our simulated results with measurements and simulations presented in [15] and [16]. The used element in unit cells was the rectangular patch. The periodicity was equal to 22 mm. In structure 1 the dimensions of the patch were w = 7 mm and L = 10 mm. In structure 2 the dimensions of the patch were w = 8 mm and L = 8 mm. The structures were built on a dielectric with $\varepsilon_r = 3.9$ and a thickness equal to 1.5 mm. in our simulations we used 6 basis functions and the number of spectral terms ranging from 200 to 10,000.

Figure 4 shows a comparison between numerical and measured results for a cascading structure. The air gap between structures was 1.5 mm. The structures are cascaded using Teflon spacers and screws to obtain the air gap. For this air gap between structures we can see that appear two resonances for our simulated results and those presented in [15]. Measured results present resonance frequencies equal to 9.07 GHz and 10.59 GHz, our simulated results present resonance frequencies equal to 8.99 GHz and 10.29 GHz, and simulated results presented in [15] present resonance frequencies equal to 9.49 GHz and 10.25 GHz. The bandwidths for measured results were equal to 298 MHz and 329

MHz, our simulated results were equal to 329 MHz and 329 MHz, and simulated results presented in [15] were equal to 517 MHz and 360 MHz. So, we obtained a better agreement with measured results for the spectral domain analysis (SDA) presented in this paper.
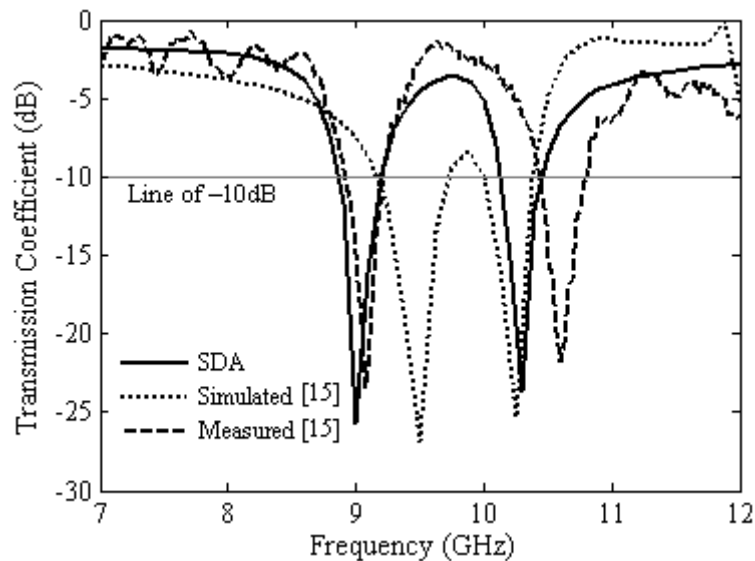

Fig. 4. Structure response for an air gap of 1.5 mm.

Figure 5 shows a comparison between numerical and measured results for a cascading structure. The air gap between structures was 3.0 mm. For this space between structures we can see that again appear two resonances for our simulated results and those presented in [15]. Measured results present resonance frequencies equal to 9.30 GHz and 10.48 GHz, our simulated results present resonance frequencies equal to 9.27 GHz and 10.89 GHz, and simulated results presented in [15] present resonance frequencies equal to 9.49 GHz and 10.25 GHz. The bandwidths for measured results were equal to 361 MHz and 596 MHz, our simulated results were equal to 361 MHz and 423 MHz, and simulated results presented in [15] were equal to 611 MHz and 267 MHz. For the first resonance our results obtained a better agreement with measured results. This also occurs for the bandwidths. The worst difference between our results and those measured in [15] for the second resonance frequency is probably due to the number of basis functions used.

Figure 6 shows a comparison between numerical and measured results for a cascading structure. The air gap between structures was 6.0 mm. The measured results were presented in [16]. For this air gap we can see that appear only one resonance. Measured results present a resonance frequency equal to 9.72 GHz, our simulated results present resonance frequency equal to 9.70 GHz, and simulated results presented in [16] present resonance frequency equal to 9.50 GHz. The bandwidth for measured results was equal to 1.83 GHz, for our simulated results it was equal to 1.24 GHz, and for simulated results presented in [16] it was equal to 1.91 GHz. We obtain a better result for resonance prediction but for the bandwidth our technique did not present a better prediction.
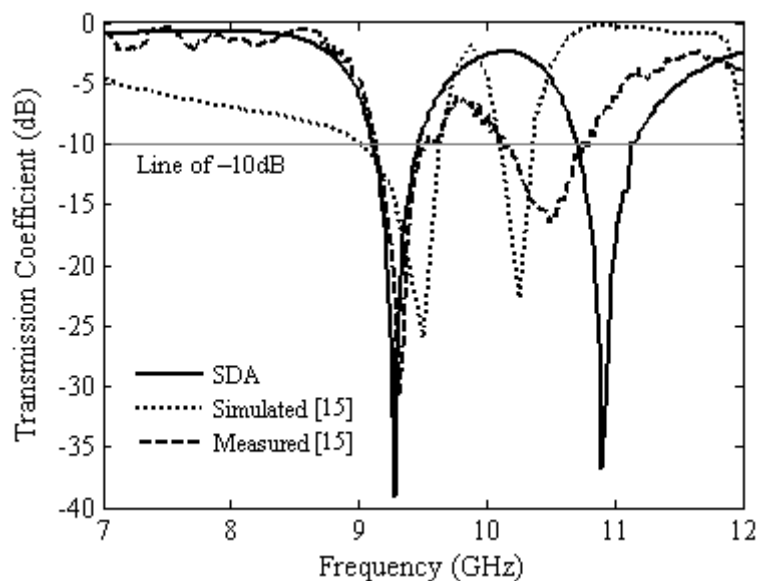
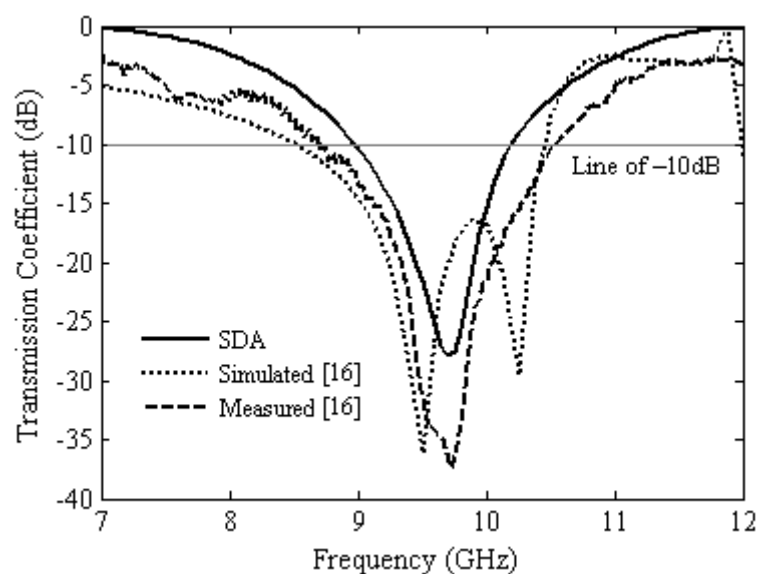Fig. 5. Structure response for an air gap of 3.0 mm.

Fig. 6. Structure response for an air gap of 6.0 mm.

Figure 7 shows a comparison between numerical and measured results for a cascading structure. The air gap between structures was 8.0 mm. The measured results were presented in [16]. For this air gap we can see that appear only one resonance. Measured results present a resonance frequency equal to 9.82 GHz, both simulated results presented in this paper and those presented in [16] obtain a resonance frequency equal to 9.50 GHz. The bandwidth for measured results was equal to 1.83 GHz, for our simulated results it was equal to 1.24 GHz, and for simulated results presented in [16] it was equal to 1.91 GHz. For this air gap the results presented in [16] obtain a better agreement with measured results.

Figure 8 shows a comparison between numerical and measured results for a cascading structure. The air gap between structures was 10.0 mm. The measured results were presented in [15]. Measured results present resonance frequencies equal to 9.31 GHz and 10.06GHz and simulated results

presented in [15] obtain resonance frequencies equal to 9.50GHz and 10.25GHz. Our results presented two resonances frequencies equal to 9.39 GHz and 10.21 GHz. For this air gap our results obtain a better agreement with measured results.
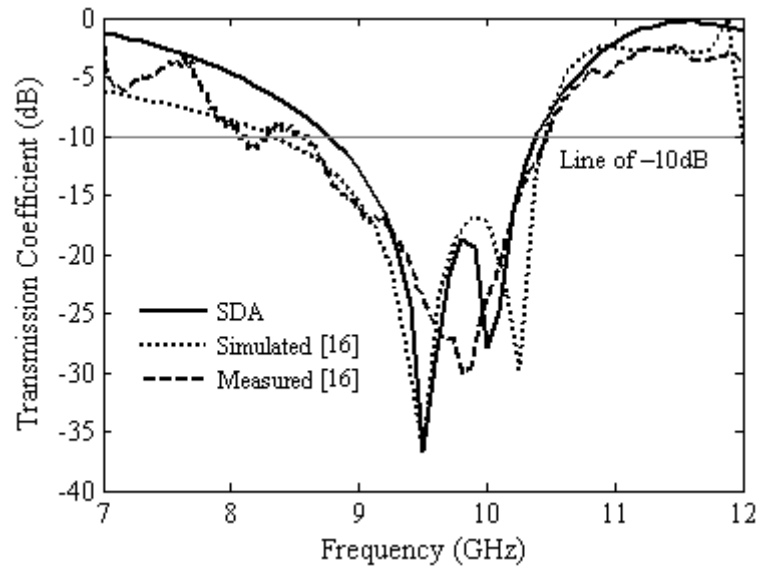

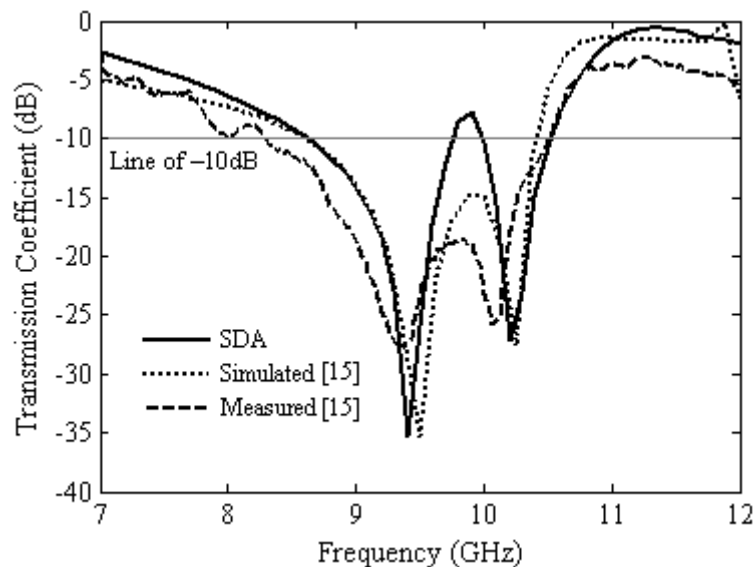Fig. 7. Structure response for an air gap of 8.0 mm.

Fig. 8. Structure response for an air gap of 10.0 mm.

Comparing the analysis performed in this work with the one developed in [15] some observations can be made. For small gaps, the analysis performed in this paper provides more accurate results. In fact, as the air gap increases the results did not differ so much. With respect to computational effort, the approximate analysis of [15] presents a high computational effort to get the results of single FSS. After this, the approximated cascading technique applied has a very low computational effort. The analysis developed in this paper

presents a high computational effort, for all structures analyzed, and is compatible with commercial computer programs as Ansoft Designer^TM and CST Studio, for example.

IV. CONCLUSIONS

The entire formulation to get the scattering of electromagnetic waves from a double screen FSS with conducting patch elements on isotropic materials was presented, in the spectral domain, for the determination of the reflection and transmission coefficients. The spectral domain immitance approach and the method of moments were used to get the characteristics of the FSS structures with patches. Numerical results obtained in this work were compared with simulations and measurements presented by another authors. For low air gap values, our results obtained a much better agreement with measurements when compared with the simulations presented in [15]. The accurate of the results is strongly dependent of the number of basis functions used in the analysis. A convergence study must be done to investigate this better.

REFERENCES

[1] B. A. Munk, "Frequency Selective Surfaces – Theory and Design", Jonh Wiley & Sons, New York, USA, 2000.
[2] T. K. Wu and S. W. Lee, "Multiband Frequency Selective Surface with Multiring Patch Elements", IEEE Transactions on Antennas and Propagation, Vol. 42, No. 11, pp. 1484 – 1490, 1994.
[3] S. B. Savia and E. A. Parker, "Superdense FSS with Wide Reflection Band and Rapid Rolloff", Electronic Letters, Vol. 38, No. 25, pp. 1688, 2002.
[4] G. Q. Luo *et al.*, "Design and Experimental Verification of Compact Frequency-Selective Surface With Quasi-Elliptic Bandpass Response", IEEE Transactions on Microwave Theory and Techniques, Vol. 55, No. 12, pp. 2481 – 2487, 2007.
[5] T. K. Wu, "Frequency selective surface and grid array", Jonh Wiley & Sons, New York, USA, 1995.
[6] T. L. Silva and A. L. P. S. Campos, "Formulation of Double Screen FSS Analysis Using Fullwave Method", International Microwave and Optoelectronics Conference, pp. 512 – 516, 2011.
[7] R. Dubrovka, J. Vazquez, C. Parini e D. Moore, "Multi-frequency and multi-layer frequency selective surface analysis using modal decomposition equivalent circuit method", IET Microwave Antennas & Propagation, Vol. 30, No 3, pp. 492 – 500, 2009.
[8] S. W. Lee, G. Zarrillo e C. L. Law, "Simple formulas for transmission through periodic metal grids or plates", IEEE Transactions on Antennas and Propagation. 30 (5), 904 – 909 (1982).
[9] T. Cwik e R. Mittra, "The cascade connection of planar periodic surfaces and lossy dielectric layers to form an arbitrary periodic screen", IEEE Transactions on Antennas and Propagation, AP-35 (12), 1397 – 1405 (1987).
[10] J. D. Vacchione e R. Mittra, "A generalized scattering matrix analysis for cascading FSS of different periodicities", International IEEE Antennas and Propagation Symposium Digest, Dallas, TX, 1, 92 – 95, 1990.
[11] J.-F. Ma e R. Mittra, "Analysis of multiple FSS screens of unequal periodicity using an efficient cascading technique", IEEE Trans. Antennas Propag. 53 (4), 1401 – 1414 (2005).
[12] R. H. C. Manioba, A. G. d'Assunção and A. L. P. S. Campos, "Improving Stop-Band Properties of Frequency Selective Surfaces with Koch Fractal Elements", International Workshop on Antenna Technology, pp. 1 – 4, 2010.
[13] A. C. C. Lima and E. A. Parker, "Fabry-Perot Approach to the Design of Double Layer FSS", IEE Proceedings, pp. 157 – 162, 1996.
[14] R. D. Nair, A. Neelam and R. M. Jha, "EM Performance Analysis of Double Square Loop FSS Embedded C-sandwich Radome**"**, Applied Electromagnetic Conference, pp. 1 – 3, 2009.
[15] A. L. P. S. Campos, R. H. C. Maniçoba_, L. M. Araújo_, and A. G. d'Assunção, "Analysis of Simple FSS Cascading With Dual Band Response", IEEE Transactions on Magnetics, Vol. 46, No. 8, pp. 3345 – 3348, 2010.
[16] R. H. C. Maniçoba, "Estudo Comparativo de Técnicas de Cascateamento de Superfícies Seletivas em Freqüência", Master Thesis, Federal University of Rio Grande do Norte, 2009.